Direct Shape Programming of Liquid Crystal Elastomers

Journal:	*Soft Matter*
Manuscript ID	SM-ART-10-2018-002174.R1
Article Type:	Paper
Date Submitted by the Author:	01-Dec-2018
Complete List of Authors:	Barnes, Morgan; Rice University, Materials Sciences and NanoEngineering Verduzco, Rafael; Rice University, Chemical and Biomolecular Engineering

Soft Matter

ARTICLE TYPE

Cite this: DOI: 10.1039/xxxxxxxxxx

Direct Shape Programming of Liquid Crystal Elastomers†

Morgan Barnes[a], and Rafael Verduzco[ab]

Received Date
Accepted Date

DOI: 10.1039/xxxxxxxxxx

www.rsc.org/journalname

Liquid crystal elastomers (LCEs) are shape morphing materials promising for many applications including soft robotics, actuators, and biomedical devices, but current LCE synthesis techniques lack a simple method to program new and arbitrary shape changes. Here, we demonstrate a straightforward method to directly program complex, reversible, non-planar shape changes in nematic LCEs. We utilize a double network synthesis process that results in a competitive double network LCE. By optimizing the crosslink densities of the first and second network we can mechanically program non-planar shapes with strains between 4 - 100%. This enables us to directly program LCEs using mechanical deformations that impart low or high strains in the LCE including stamping, curling, stretching and embossing methods. The resulting LCEs reversibly shape-shift between the initial and programmed shape. This work widens the potential application of LCEs in biomedical devices, soft-robotics and micro-fluidics where arbitrary and easily programmed shapes are needed.

1 Introduction

Liquid crystal elastomers (LCEs) are polymeric networks that exhibit large and reversible shape changes in response to a variety of stimuli including heat, UV or near-IR light and magnetic or electric fields[1–8]. These materials are promising as actuators and for applications in soft robotics[9–25]. However, current synthesis and processing methods limit the fabrication of LCEs with complex, arbitrary shape changes.

LCE shape changes are governed by a coupling between the liquid crystal director and the anisotropic polymer network. Monodomain nematic LCEs with a uniform alignment of the liquid crystal director can be prepared via uniaxial mechanical extension during synthesis. By heating the sample beyond the nematic-to-isotropic transition temperature T_{NI}, the system transitions from the state programmed in the nematic phase to that programmed in the isotropic state.[26–28]. Such monodomain LCEs reversibly change shape with heating and cooling due to changes in the liquid crystal order parameter, which is coupled to the network anisotropy[29]. Contraction and elongation, curling, and surface wrinkling have been reported using mechanically aligned monodomain LCEs and LCE bilayers[4,30–33].

More diverse shape changes in LCEs can be achieved by imprinting complex nematic director orientations. For example, elaborate director orientations and liquid crystal images can be imprinted into LCEs using patterned surfaces to produce a range of shape responses including splay, conical structures, and Gaussian curvatures[6,34–43]. Additive manufacturing has also been recently employed to produce LCEs that can transition between two non-planar shapes[44,45]. A complication of these methods is that they generally require solving the inverse problem of determining the necessary liquid crystal director profile to produce a desired shape change[41,46–48]. Further, the use of patterned surfaces relies on surface forces, limiting the technique to thin, flat samples. Other approaches include simultaneously stretching the LCE in different directions to mechanically align a specific director profile[49] or curling and crosslinking a stretched monodomain LCE.[50]. The approach of curling and crosslinking a monodomain LCE opens up a method for arbitrarily programming curvatures in LCEs with some limitations in the strain range possible and necessity for starting with a uniaxially oriented LCE.[50]

Here we investigate an alternative and straightforward method to program complex three-dimensional shapes in nematic LCEs by mechanically deforming the LCE into a desired non-planar shape during a double network synthesis process, as shown in Figure 1. The resulting LCE should reversibly transition between the shapes programmed during the first and second network crosslinking reactions. A challenge of implementing this approach is that non-planar mechanical deformations such as curling produces low ($< 10\%$) strains, while stretching produces much larger (100%)

[a] Department of Materials Science and NanoEngineering, Rice University, Houston, Texas 77005, USA. E-mail: RafaelV@Rice.edu
[b] Department of Chemical and Biomolecular Engineering, Rice University, Houston, Texas 77005, USA.

† Electronic Supplementary Information (ESI) available: [details of any supplementary information available should be included here]. See DOI: 10.1039/cXsm00000x/

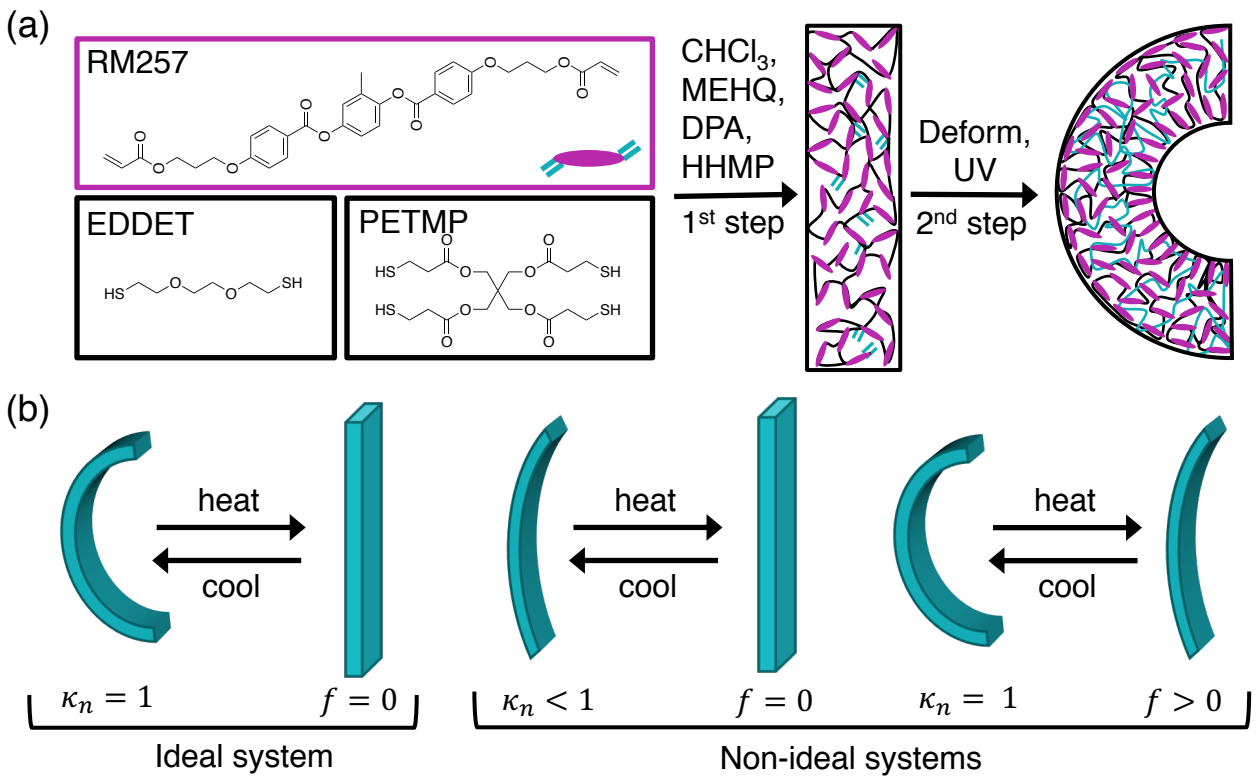

Fig. 1 (a) Schematic for the preparation of LCEs including the resulting liquid crystal alignment. The curvature causes parallel alignment of the liquid crystals at the outer edge due to tensile forces. Perpendicular alignment occurs at the inner edge due to compressive forces and could either be in plane, as depicted, or into the page. (b) Schematic illustrating the ideal and non-ideal shape changes of fully cured LCEs and their respective normalized curvature, κ_n, and flatness, f values.

strains. The LCE network chemistry should be optimized to be able to lock-in deformations over this entire strain range.

The concept of a competitive double network structure is useful to guide optimization of the LCE to achieve reversible shape programming. In a typical LCE synthesis, the first network is cured in the isotropic state, deformed by mechanically loading the sample, and then cured again in the nematic state. LCEs fabricated using this general approach are an example of double network elastomers, which have been studied for over 50 years.[51–55] A general feature of double network elastomers is that the final state of the dual-cure elastomer retains some fraction of the strain applied during the second crosslinking reaction and is dependent on the relative crosslink densities or moduli of the first and second network crosslinking reactions.[56,57] This concept of a double network structure has also been applied to double network shape memory polymers where the elastic restoring force of the first network must be balanced with the strength of the second network to enable reversible[58] and irreversible shape changes[59,60].

In the case of a double network LCE, we hypothesized that finding the proper balance between the first and second networks would be necessary to achieve reversible shape programming compatible with a wide range of sample strains. Below, we demonstrate optimization of the LCE network composition by systematically varying the network composition of the first and second crosslinking steps to produce LCEs that can transition between a mechanically programmed bend deformation and fully recover their initial shape on heating. We show that the resulting optimized LCE can be used to mechanically program shapes with strains in the range of 4 - 100 %, and we demonstrate programming and reversible shape changes using curling, stamping, stretching, and embossing methods. This method necessitates no foresight of the required director profile and is not limited to initially flat films. The resulting LCEs can shape-morph between three-dimensional topologies and reproduce shapes and textures with low- and high-strain deformations.

The demonstrated method of mechanically deforming a material to produce a desired shape change is similar to those commonly used to program shape memory polymers (SMPs). In a SMP a temporary shape is directly imprinted in a polymer at elevated temperatures and remains after the materials is quenched.[61–63] When the SMP is heated the original shape is recovered and the programmed shape is generally lost unless it is reprogrammed. Our work combines the straightforward shape-programming in SMPs with the full shape-reversibility of LCEs.

2 Experimental Methods

Materials and Methods

2,2'-(ethylenedioxy) diethanethiol (EDDET), pentaerythritol tetrakis (3-mercaptopropionate) (PETMP), 1,4-Bis-[4-(3-acryloyloxypropyloxy)benzoyloxy]-2- methylbenzene (RM257), chloroform, dipropyl amine (DPA), 4-methoxyphenol (MEHQ), and (2-hydroxyethoxy)-2-methylpropiophenone (HHMP) were

obtained from commercial suppliers and used as received.

Synthesis

LCEs are made following a previously reported double network thiol-acrylate polymerization[28]. RM257 is the liquid crystal monomer and is a chain extender for the first network and the crosslinker in the second network. EDDET and PETMP acts as a flexible chain extender and crosslinker for the first network, respectively. A series of LCEs that varied in PETMP and excess acrylate contents were prepared using the same general procedure. The following procedure is for an LCE with 10 mol % excess acrylate and 25 mol % of the thiols coming from PETMP. First, RM257 (300 mg, 0.510 mmol), 0.5 wt % HHMP (1.5 mg), and 0.25 wt % MEHQ (0.75 mg) are dissolved in chloroform (120 mg) at 70°C. MEHQ is added to prevent unintentional acrylate-acrylate polymerization before UV-curing. After the mixture has cooled to room temperature EDDET (63.31 mg, 0.348 mmol) and PETMP (28.29 mg, 0.058 mmol) are added followed by a 2 wt % DPA solution in chloroform (46.26 mg, 0.009 mmol, 1 mol %). The masses of reagents used to synthesize other compositions are listed in Supplementary Information Table S1 and the chemical reaction scheme is reported in Supplementary Information Scheme S1. The mixture is then vortexed to ensure proper mixing and placed under vacuum to remove any bubbles. Next, the mixture is deposited into the desired mold and cured for at least 5 hours. After the first cure is complete the LCE is heated to 80 °C under a vacuum of 30 mm hg for 5 hours to remove the chloroform. Finally, the LCE is mechanically deformed to the desired shape and irradiated with 365 nm light for 10 minutes to complete the second cure step. Additional details on the molds used for the first cure step and methods for deforming the LCEs during the second cure step are included below.

Imaging and Image analysis

Cross-polarized optical images were taken using a Zeiss Axioplan 2 microscope. A curved LCE was imaged through its thickness with the polarizers at 0 and 45 angles from the outer edge. The gray scale images were subtracted from each other to obtain the intensity change image. All three images were then mapped to the same color scale to illustrate intensity differences.

Programmed LCEs were imaged using an iPhone camera with the color levels adjusted to enhance contrast with the background.Python and OpenCV were used for all image analysis. To determine normalized curvature and flatness, blackened samples were imaged against a white background at room temperature. A circle was fitted to the outer edge of the digital sample image, and the normalized curvature κ_n was calculated using Equation (1),

$$\kappa_n = \frac{\rho_{cure} + t}{\rho_{LCE}} \quad (1)$$

where ρ_{LCE} is the radius of curvature of the LCEs outer edge, ρ_{cure} is the radius of curvature of the rod used in the second cure, and t is the thickness of the LCE.

To calculate flatness, the samples were imaged at 150°C, which is well above the T_{NI} for all samples. A line was fitted to the midpoint between the detected edges of the digital image, and a standard error was calculated to determine flatness f using Equation (2),

$$f = \sqrt{\frac{\Sigma(Y - Y')^2}{N}} \quad (2)$$

where Y is the mean value of the LCEs outer and inner edges at a specific position, Y' is the fitted line value at that position, and N is the number of position sampled along the sample length.

Table 1 Compositions and thermal properties of LCE samples prepared. PETMP Thiol content is the mol % of thiol functional groups from PETMP, and excess acrylate is the mol % excess of acrylate functional end groups relative to thiol functionalities. T_g and T_{NI} determined using differential scanning calorimetry.

PETMP Thiol Content (%)	Excess Acrylate (%)	T_g (°C)	T_{NI} (°C)
10	5	1.93	84.21
	10	-0.27	83.52
20	5	0.33	79.90
	10	-1.89	79.33
	15	-1.82	81.40
25	5	2.39	85.10
	10	0.49	79.64
	15	2.35	86.73
40	5	6.5	78.21
	15	3.98	84.78
	25	-1.23	86.26
60	5	11.62	80.12
	15	8.86	90.11
	25	4.18	89.62
80	5	14.95	91.09
	15	16.2	91.21
	25	8.94	87.65

Two-Dimensional Wide Angle X-Ray Scattering (WAXS)

Liquid crystal orientation and order parameter were calculated using a Rigaku Diffractometer using a RUH3R Copper Target Rotating Anode with a wavelength of 0.154 nm, phi axis goniometer with vertical orientation, and a Rigaku R-Axis IV++ Image Plate Area Detector. The detector imaging area is approximately 380 mm X 380 mm, with a distance of 300 mm between the sample and detector. The order parameter was calculated numerically with Python using Equation (3) from Deutsch et al.[64,65]

$$S = 1 - N^{-1}\frac{3}{2}\int I(\theta)\left[sin^2\theta + \left(sin\theta cos^2\theta\right)Log\left(\frac{1+sin\theta}{cos\theta}\right)\right]d\theta \quad (3)$$

where $N = \int I(\theta)d\theta$.

Differential Scanning Calorimetry

The glass transition, T_g, and nematic to isotropic transition temperature, T_{NI}, were determined using TA instruments Q20 differential scanning colorimeter (DSC). LCEs were analyzed prior to

the second curing step because the T_{NI} is not detectable by DSC after the second cure step.[28] Samples were equilibrated to -20 °C for 5 minutes and then heated at a rate of 5°C/min to 100°, held at that temperature and for 5 minutes and then cooled to -20 °C at a rate of 5 °C/min. The cycle was repeated once more and T_g and T_{NI} were determined from the second heating cycle as the stepwise decline and endothermic well in the heat flow, respectively.

Dynamic Mechanical Analysis

Young's moduli were obtained using an ARES G2 (TA instruments) rheometer using a linear film tension clamp. Rectangular samples were loaded into the clamp and pulled at a Hencky strain rate of 5 %/min. Young's modulus is calculated as the slope of a line fitted to the stress-strain curve from 0 to 1.5% strain.

Actuation and Fixity

Fixity and actuation were determined by first placing two marks a distance of 10 mm apart on a rectangular LCE that has undergone the first network crosslinking reaction. The length of the sample at this stage is denoted the initial length l_o. The sample was then stretched to a desired strain (e.g., 20 mm for 100% cure strain), UV cured for 10 minutes, heated above the T_{NI}, and then cooled back to room temperature.

The distance between the marks was measured in both the elongated state (room temperature) and contracted state (above T_{NI}) to determine the elongation and contraction fixities. Elongation fixity is the ratio of the elongated length, l_e, to the cured length, l_{cure}, and contraction fixity is the ratio of the contracted length, l_c to the initial length, l_0. The actuation strain, $\varepsilon_{actuation}$, and normalized actuation strain, $\varepsilon_{normalized}$, were calculated using Equations (4) and (5),

$$\varepsilon_{actuation} = \frac{l_e - l_c}{l_c} * 100 \tag{4}$$

$$\varepsilon_{normalized} = \varepsilon_{actuation} * \frac{l_0}{l_{cure} - l_0} * 100 \tag{5}$$

where $\varepsilon_{normalized}$ is $\varepsilon_{actuation}$ normalized by the cure strain.

LCE Programming

All fabrication molds and stamps can be found in the Supplementary Information Figure S1. The LCE face, four pillar structure, and Rice logo were all fabricated using an embossing method. LCEs were initially cured between two glass slides with spacers to yield a desired thickness. The LCE was then pressed between a positive and negative mold of the same object, placed in a freezer for 10 minutes to prevent sticking to the mold, removed from the mold and cured for 10 minutes under 365 nm UV light.

The face was made using a purchased silicone mold of the negative face, and the positive image was created from pressing Sculpey oven bake clay into the silicone cavity. The clay was then baked 15 minutes at 130 °C for every 1/4 inch of thickness. The four-pillar structure was fabricated in a similar fashion, with a LEGO®piece as the positive image and the pressed clay as the negative.

The Rice logo was created using a Universal X-660 laser cutter. The logo was cut into 3/32-inch-thick basswood. The positive and negative logos were glued onto basswood substrates to create the positive/negative stamps.

The wave LCE was made using a polydimethylsiloxane (PDMS) mold. First, clay was flattened to uniform thickness (1 mm) and hand curved into a wave structure. The clay was placed upright in a plastic container and uncured PDMS was poured around the clay and cured at room temperature for 24 hours. Then the PDMS was removed from the container, cut in half, and the clay was removed. The PDMS mold was placed back in the container, and LCE solution was poured into the cavity and cured, removed, and dried. The wave LCE was then flattened, curled around a rod, and UV cured.

The quarter LCE was made by lightly hand pressing an initially flat LCE against the back surface of a quarter. The LCE was then removed from the quarter and UV cured. The flower was made by cutting a petaled spiral out of a, initially flat LCE and hand rolling it into a flower and UV cured. Additional programmed LCEs are shown in the Supplementary Information Figure S2.

3 Results and discussion

Our first objective was to optimize the LCE network composition by quantifying the ability of an LCE to hold a curled shape and reversibly transform to a flat sheet, as illustrated in Figure 1. Ideally, the LCE should fully and reversibly transition between the flat and curled shapes, as shown schematically in Figure 1b. We hypothesized that this could be achieved by optimizing the compositions of the first and second network.

The double network chemistry chosen to prepare LCEs enables systematic modulation of the crosslink densities of the first and second networks through variation of the PETMP content and relative excess of the acrylate functional groups to thiols. The PETMP content determines the degree of branching and crosslinking in the first network while the excess acrylate content influences the crosslink densities of both the first and second networks. The network composition has only a modest impact on the glass-transition temperature, T_g, and nematic-to-isotropic transition temperature, T_{NI}, as shown in Table 1. The T_g increases with PETMP content, and T_{NI} is not greatly affected by these variations in network composition. This is consistent with prior studies of similar LCE networks.[66]

As shown in Figure 2a, the modulus of LCEs always increases between the first and second crosslinking steps, as expected. Also, increasing the PETMP content generally increases the final modulus after both network crosslinking steps. This is expected because a higher PETMP content increases network branching and crosslink density. Finally, increasing the excess acrylate content decreases the modulus of the first network and increases the modulus of the second network, producing a much larger jump in modulus between first and second crosslinking steps at higher acrylate contents.

To quantify the ability of the LCEs to hold a programmed curvature and return to a flat sheet when heated above T_{NI}, an initially flat polydomain LCE was wrapped around a rod with a known radius of curvature and photo-cured to define the second net-

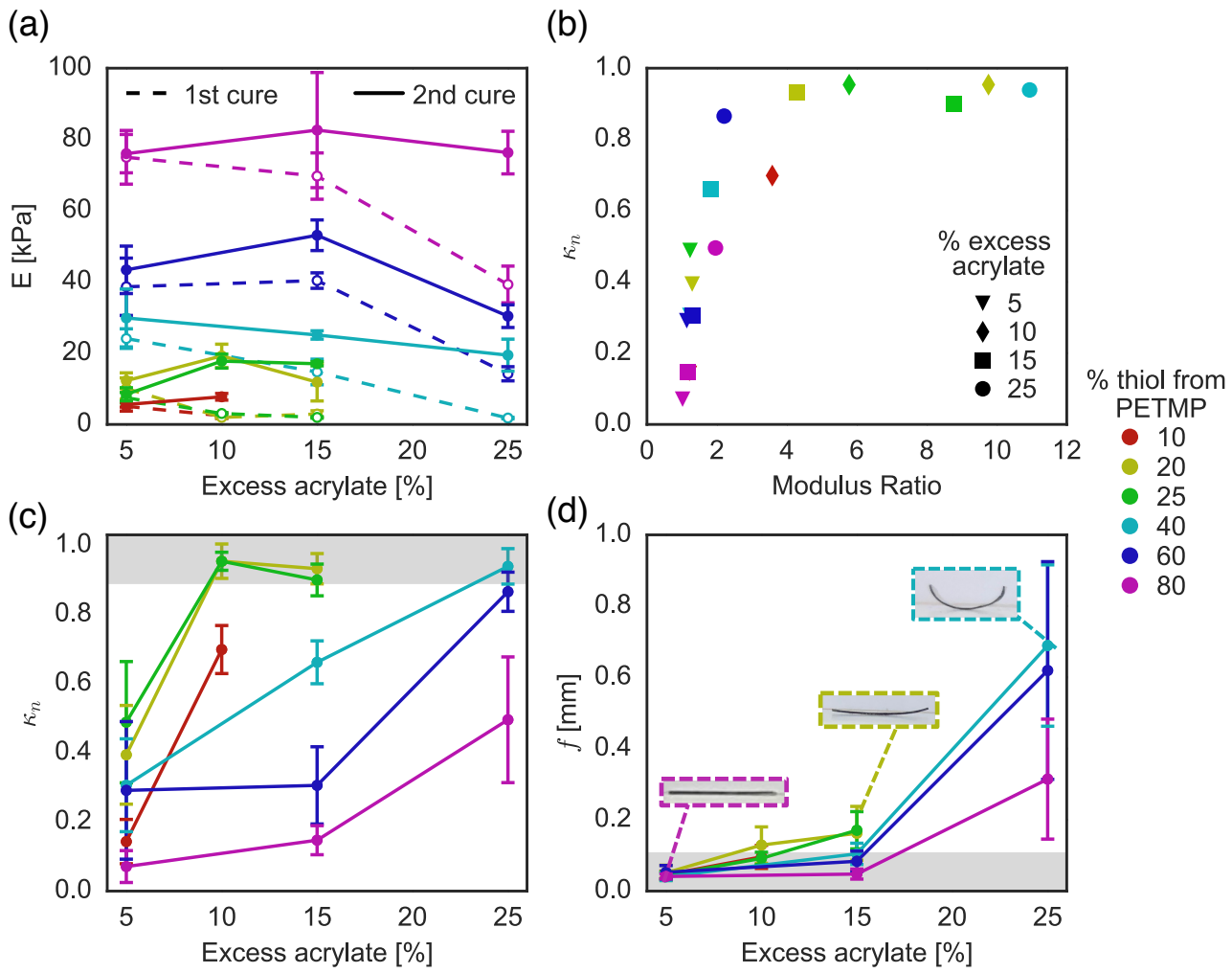

Fig. 2 (a) LCE Young's moduli after the first and second network crosslinking reactions. (n = 3, error bars indicate 95% confidence intervals of the mean) (b) The mean normalized curvature, κ_n as a function of the ratio of Young's moduli after the 2nd cure relative to the 1st cure. (c, d) Normalized curvature, κ_n, and fatness, f, of LCEs ($t \approx 250$ μm) photo-cured around a rod ($\rho = 2.455$ mm). Grey regions indicate samples that maintain their programmed curvature at room temperature and flatten when heated. (n = 15, error bars indicate 95% confidence intervals of the mean). Numerical data is reported in Supplementary Information Table S2.

work and lock-in the curled shape. Residual stresses were then removed by subjecting each sample to one heating and cooling cycle above T_{NI} ($\approx 75-90$ °C). We then measured the normalized curvature κ_n and flatness parameter f for each sample. The normalized curvature κ_n is the ratio of the programmed to actual radius of curvature at room temperature. The flatness parameter f is the standard error for a linear fit to a cross-sectional image of the LCE at temperatures above T_{NI}. Details on the measurement and determination of κ_n and f are provided in the Experimental section. In the ideal scenario where an LCE holds the programmed curvature at room temperature and returns to a perfectly flat sheet on heating above T_{NI}, $\kappa_n = 1$ and $f = 0$.

As shown in Figure 2b, the ability for an LCE to hold its programmed curvature is strongly influenced by the ratio of the Young's moduli after the first and second curing steps. The normalized curvature increases with the modulus ratio, indicating that a progressively stronger second network is better able to hold the curled shape. This supports the picture of a competitive double network structure and provides a simple metric for determining whether a particular composition will lead to LCEs that can retain a programmed shape.

The dependence of κ_n on the excess acrylate and PETMP contents is shown in Figure 2c and demonstrates that LCEs are able to retain the programmed shape only for sufficiently high excess acrylate contents. κ_n increases from 0 to 1 with increasing excess acrylate content for all LCEs. Increasing the PETMP content, which results in a higher crosslink density of the first network, generally results in a decrease in κ_n. This demonstrates that too high of a crosslink density in the first network or too low of a crosslink density in the second network is detrimental to shape programming. At a very low PETMP thiol content of 10 %, programming a curled shape is also unsuccessful, which we attribute to the poor mechanical properties of the first network and weak coupling between the network and nematic director during shape

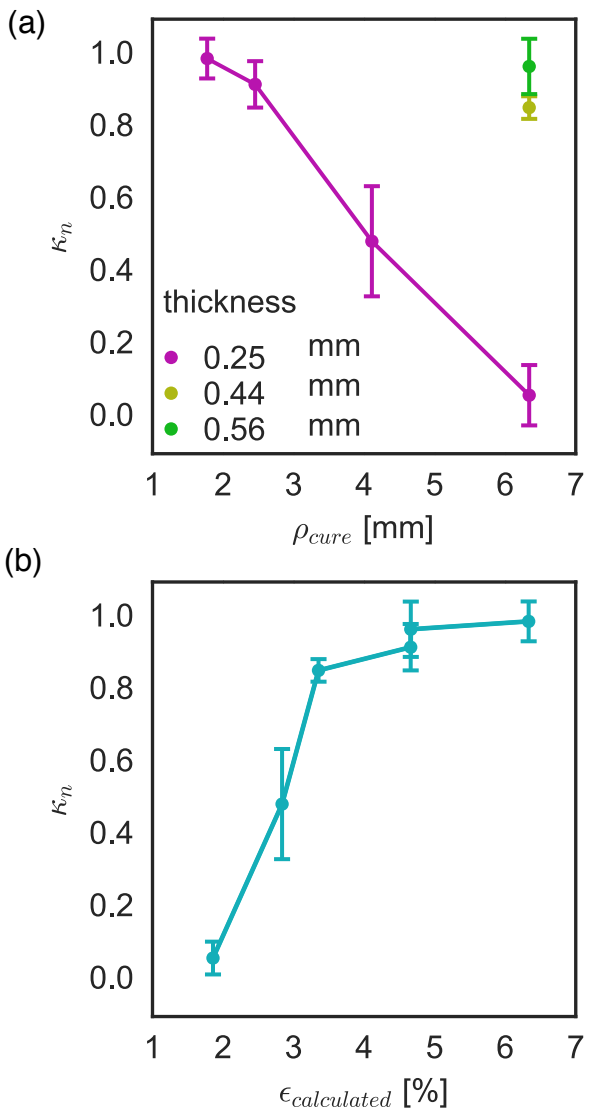

Fig. 3 (a) Normalized curvature as a function of radius of curvature, ρ_{cure}, and sample thicknesses, t, and (b) as a function of calculated maximum strain, $\varepsilon_{calculated} = t/(2\rho_{cure})$, in the LCE. (n = 5, error bars indicate 95% confidence intervals of the mean) Numerical data is listed in Supplementary Information Table S3.

programming.

The data shown in Figure 2d demonstrate that LCEs can return to a flat sheet on heating ($f < 0.125$ mm) only below a threshold excess acrylate content. At too high of an excess acrylate content, the second network dominates and the LCE retains a curled shape at temperatures above the T_{NI}. Furthermore, increasing the PETMP content results in an increased crosslink density of the first network and a smaller value of f, indicating a flatter LCE sheet at elevated temperatures.

Altogether, these studies demonstrate that a balanced composition and crosslink densities of the first and second networks are needed to achieve the programmed curvature and return to a flat LCE sheet on heating. κ_n values near 1 are associated with relatively strong second networks and larger excess acrylate contents, while low f values are associated with a relatively strong first network, which corresponds to lower excess acrylate and higher PETMP contents. The optimal composition range for an LCE that can both hold its mechanically programmed curvature ($\kappa_n \approx 1$) and return to its initial shape ($f < 0.125$ mm) is indicated in the shaded regions of Figures 2c and d. The samples that fall in the optimal range for both $\kappa_n \approx 1$ and $f \approx 0$ contain approximately 25 % PETMP content and 10 % excess acrylate. This composition of LCE is used in shape programming studies described below.

While a correct balance between the first and second networks is necessary to enable shape programming, it is also critical that the deformation re-orients the liquid crystal director in order to program a desired shape. Prior studies with LCEs have shown that mesogens align parallel to tensile forces and perpendicular to compressive forces.[26,67] Therefore, curling an LCE results in parallel alignment of the nematic director along the outer edge

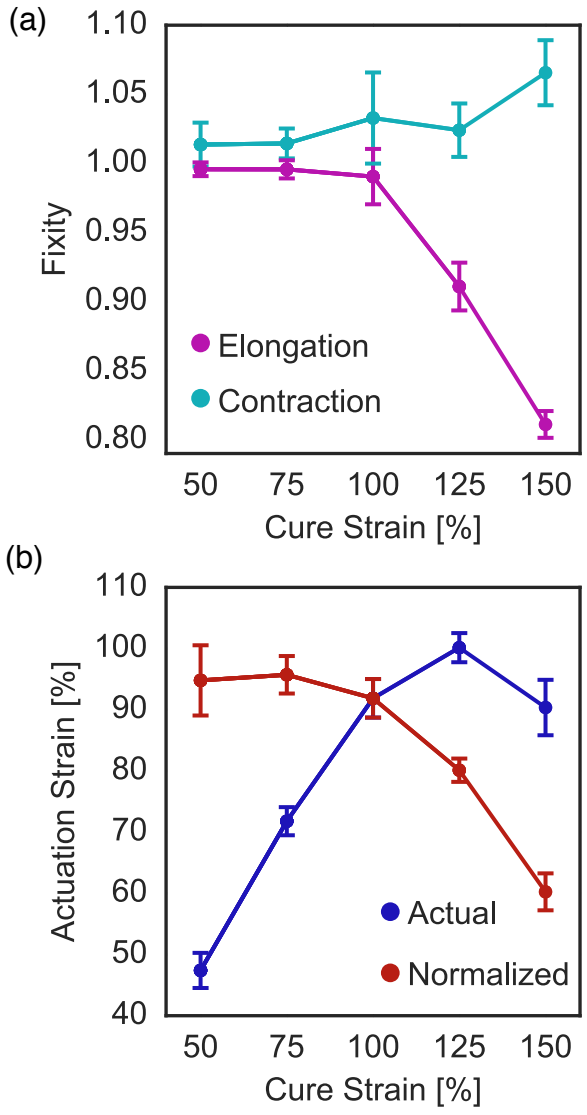

Fig. 4 (a) Elongation and contraction fixity, and (b) Actual and normalized actuation strain as a function of cure strain. (n = 5, error bars indicate 95% confidence intervals of the mean) Numerical data is reported in Supplementary Information Table S4.

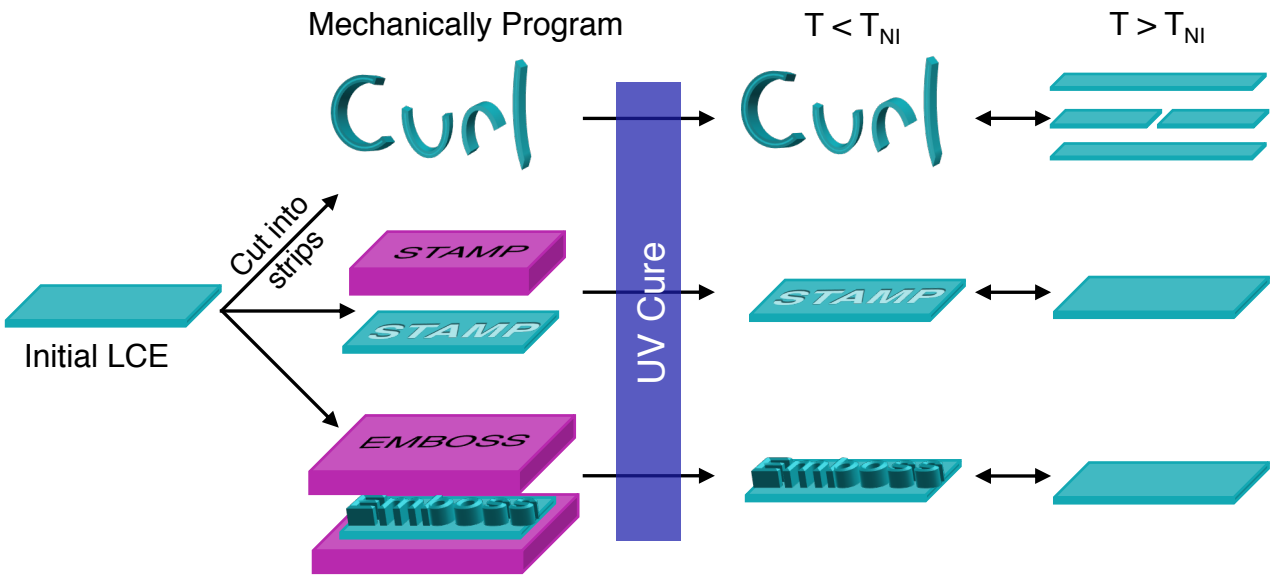

Fig. 5 Schematic detailing how LCEs are mechanically programmed via curling, stamping or embossing to achieve reversible shape-shifting between the initial and programmed shapes.

and oblate perpendicular alignment along the inner edge due to tension and compression, respectively. This is demonstrated in schematically in Figure 1a and in the cross-polarized micrographs in Figure S3 which show a curled LCE imaged through its thickness. For a perfectly uniaxially aligned LCE the cross-polarized images would show a dark image when the polarizes are parallel and perpendicular to the director. As the polarizers are rotated the image would brighten to a peak intensity when the polarizes are angled 45 relative to the director. An unaligned LCE would show no intensity difference between the two images. The intensity difference between the micrographs in Figure S3 occur along the inner and outer edge suggesting that there is partial alignment of the liquid crystal director along those edges. Only partial alignment is expected due to the low strain applied during deformation.

We sought to determine the minimum strain that could be used to successfully re-orient and shape-program the LCE. For a curling deformation, the largest strains occur on the outer and inner edges of the sample, which experience tension and compression, respectively. The maximum strain ε_{max} increases linearly with thickness and inversely with radius of curvature: $\varepsilon_{max} = t/(2\rho)$, where t is the LCE thickness and ρ is the radius of curvature assuming a neutral axis of bending at $t/2$. To determine the minimum necessary strain, we measured κ_n as a function of both the sample thickness t and curling radius ρ. As shown in Figure 3, κ_n decreases with larger ρ and with decreasing t, as expected due to decreasing sample strain. Plotting κ_n against the calculated maximum strains in Figure 3b, we find that a strain of roughly 4 % is sufficient to program a desired curved shape; κ_n is greater than 0.9 for strains of 4 % or higher.

We also determined the maximum strain that could be mechanically shape-programmed in LCEs using uniaxial extension. After the first crosslinking reaction, LCE samples were uniaxially stretched and UV-cured at varying linear strains. The elongational and contraction fixities were quantified as described in the Experimental section. The elongational and contraction fixities reflect the amount of strain that can be programmed in an LCE and the amount of residual strain that remains relative to the initial length on heating the LCE above the T_{NI}, respectively. Figure 4a shows that both the elongation and contraction fixities remain near the ideal value of 1 up to a cure strain of 100%. Above 100% cure strain the contraction fixity increases, reflecting an increasing residual strain in the sample above the T_{NI}. The elongational fixity also decreases, which shows that the the LCE does not fully lock-in the elongation applied during shape programming. The actuation strains of the samples are shown in Figure 4b showing a strong decrease in the normalized actuation strains for cure strains greater than 100 %. The actuation strain peaks at a value near 100 % for a cure strain of 125 %.

Practically, this means that strains between 4% and 100% can be adequately programmed using our optimized LCE network, but below or above these amounts the LCE will neither fully return to its initial shape nor will maintain its programmed shape. Knowing these lower and upper strain bounds is useful for designing LCE shapes. To achieve small, tight curvatures, it will be best to use thin LCEs that do not exceed 100% strain when deformed. On the other hand, thicker LCEs are required for programming shapes with broad features and large curvatures so that the imparted strain does not fall below 4%. However, care should be taken when increasing the thickness of the LCEs to ensure complete removal of solvent from the the LCE before programming and that the LCE can be adequately UV cured through the thickness.

To quantify director alignment as a function of strain applied, we obtained 2D wide-angle X-ray scattering (WAXS) measurements of LCEs that were UV cured after applying uniaxial strains

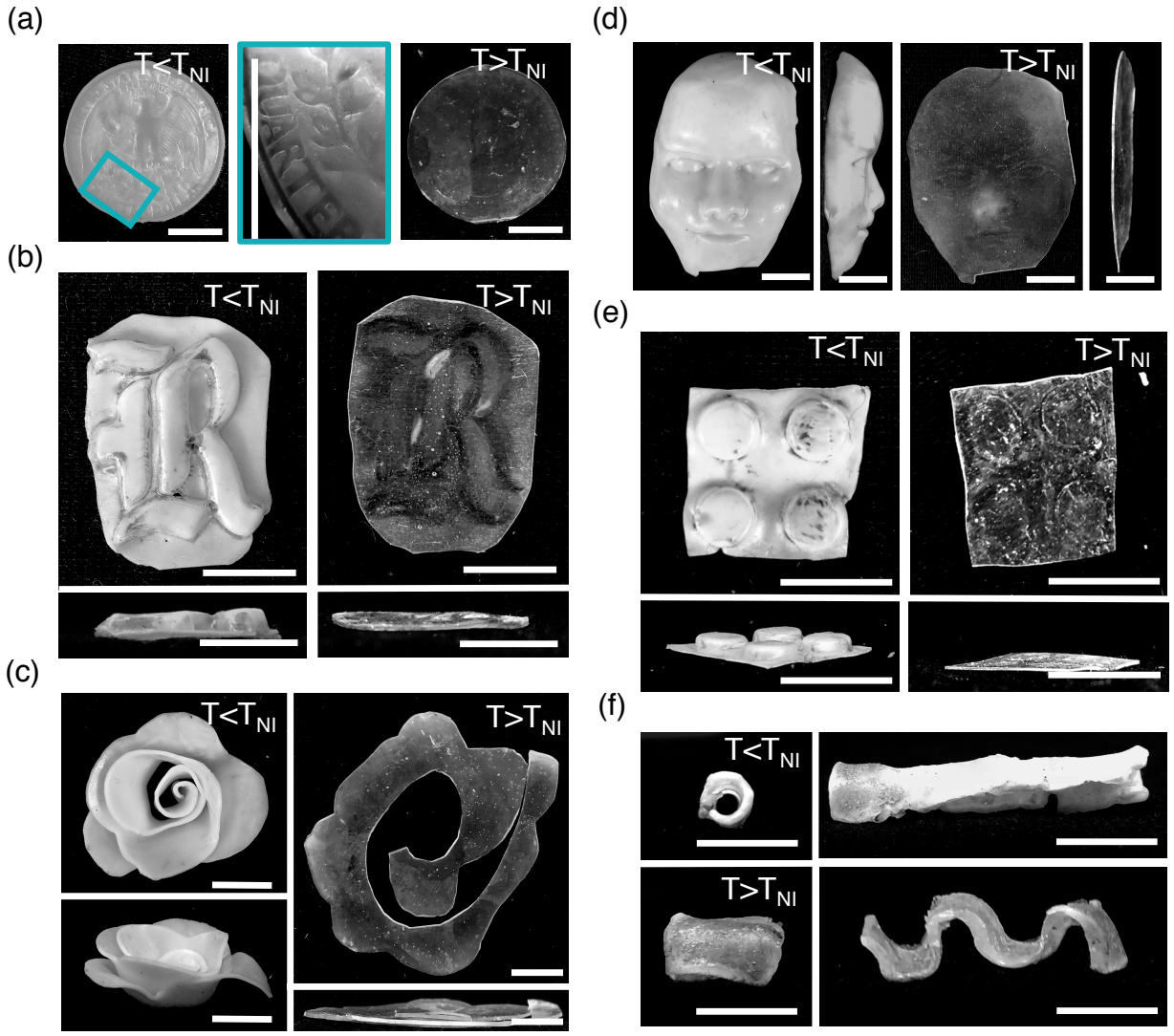

Fig. 6 Photographs of shape-programmed LCEs at $T < T_{NI}$ and $T > T_{NI}$. (scale bars = 10 mm) (a) Initially flat LCE ($t = 0.25$ mm) stamped with a quarter and cured, with an enlarged region shown in blue. (Mirror images are shown) (b) Initially flat LCE ($t = 0.25$ mm) embossed with a Rice University logo, and cured. (c) Initially flat LCE ($t = 0.45$ mm) that was cut, hand curled into a flower, and cured. (d) Initially flat LCE ($t = 0.45$ mm) pressed into a silicone mold of a face and cured. (e) Initially flat LCE ($t = 0.25$ mm) embossed with a Lego®, and cured. (f) LCE wave ($t = 1$ mm) that was flattened, curled around a rod and cured.

ranging from 0% to 150% (see Supplementary Information Figure S4). At and above 25% cure strains, WAXS patters show a clear anisotropy in the director orientation, reflecting a strain-induced alignment parallel to the stretching direction. The anisotropy and macroscopic order parameter increase with strain up to 100%, beyond which the order parameter plateaus at a maximum value of 0.66. At lower strains (5%-15%) a clear anisotropy is not evident in the 2-D WAXS patterns. This reflects weak alignment of the nematic director. The nematic director is only weakly ordered at these strains. LCEs shape programmed over this low strain range still appear hazy due to the low degree of director alignment. Plotting the diffracted intensity over all angles reveals some anisotropy that increases with strain (see Supplementary Information Figure S4). As shown in Fig. 3b, this weak anisotropy is sufficient to produce very low strains associated with curling, and being able to program low-strain deformations is important for producing topographical images, as demonstrated below.

To further verify that liquid crystal ordering was necessary to achieve reversible shape programming, we also synthesized LCEs where the second crosslinking step was conducted at temperatures above the T_{NI}. Samples were curled, heated, and UV cured at temperatures above the T_{NI}. The resulting LCEs exhibited some residual curling in the isotropic phase but with less curvature than that applied during curing. When cooled, the sample transitioned to the nematic phase and the LCE unpredictably morphed into a pretzel shape as shown in Supplementary Information Figure S5. It is unclear what drives this shape change to the pretzel configurations, but this demonstrates that liquid crystal ordering plays an important role in shape programming and is necessary for mechanical programming of reversible shape changes in LCEs.

Applying the optimized double network chemistry and knowledge of the threshold strain for shape programming enabled us to

program a variety of complex shapes through curling, stamping, and embossing as demonstrated in Figure 5. This general technique of mechanically programming complex, non-planar shapes can be extended to virtually any shape or texture, including LCEs that are not initially flat. A variety of molds and textures used to program shape changes in LCE are shown in the Supplementary Information Figure S1.

First, a topographical replication of a quarter was produced. (250 μm thick, Figure 6a) When the LCE is heated above T_{NI} it returns to a its initial smooth surface, and upon cooling the topographical features re-appear.

The embossed Rice University logo and Lego®LCEs (250 μm thick) can fully transition between their initial and programmed shapes. While some residual liquid crystal alignment can be observed, the topography disappears above T_{NI}. (Figure 6b,e and Supplementary Information Video S1,2)

The flower LCE could reversibly curl from a flat film into a flower (450 μm thick, Figure 6c, Supplementary Information Video S3).

A topographical map of a face is capable of reversibly shifting between a flat film and 3D face. (450 μm thick, Figure 6d, Supplementary Information Video S4). A thicker LCE (0.45 mm) was required to reproduce the face to capture the broad features of the face such as the forehead and cheeks which are associated with very low strains. For thinner LCEs, the strains associated with these features are insufficient to align and shape-program the LCE. A comparison of imprinting the face into thin and thick LCE samples is presented in the Supplementary Information Figure S6 to demonstrate this comparison.

Finally, to demonstrate the capability to program reversible shape changes between two non-planar shapes, an LCE retained the initially cured wave shape for elevated temperatures, and for temperatures below T_{NI} assumed an elongated, curled conformation. (1 mm thick, Figure 6f, Supplementary Information Video S5)

These examples illustrate the ease and versatility of directly programming LCE shape changes using various mechanical deformation techniques. Other examples include an LCE that transitions between a sheet with bumps and a flat sheet (Supplementary Information Figure S2b and Supplementary Information Video S6), and an LCE that transitions between textured flat LCE sheet and an LCE with a series of steps (Supplementary Information Figure S2a and Supplementary Information Video S7) Further details and additional images of programmed LCEs are included in the Supplementary Information.

4 Conclusion

In summary, we demonstrate the ability to directly program complex reversible curvatures into LCEs using mechanical deformations. By carefully optimizing the LCE network composition, a variety of complex shapes can be programmed through curling, stamping, stretching, and embossing, and the method is not limited to initially flat LCEs. This work demonstrates that concepts that have been developed for isotropic double network elastomers are applicable and useful for optimzation of shape changes in LCEs. This work also widens the potential application of LCEs in biomedical devices, soft-robotics and micro-fluidics where arbitrary and easily programmed shapes are needed. Future work using this method includes imprinting microchannels for microfluidic devices, topological pixels for braille displays or dynamic buttons, and 3D printing complex structures where the print path is not constrained to desired alignment profiles.

Conflicts of Interest

The authors declare no competing financial interests.

Acknowledgements

The authors acknowledge support from the Welch Foundation for Chemical Research (C-1888), the Army Research Office Chemical Sciences Division (W911NF1810289), and the Shared Equipment Authority at Rice University.

References

1 T. J. White and D. J. Broer, *Nat. Mater.*, 2015, **14**, 1087–1098.
2 M. Wang, S. M. Sayed, L. X. Guo, B. P. Lin, X. Q. Zhang, Y. Sun and H. Yang, *Macromolecules*, 2016, **49**, 663–671.
3 Y. Yang, W. Zhan, R. Peng, C. He, X. Pang, D. Shi, T. Jiang and Z. Lin, *Adv. Mater.*, 2015, **27**, 6376–6381.
4 C. Yuan, D. J. Roach, C. K. Dunn, Q. Mu, X. Kuang, C. M. Yakacki, T. J. Wang, K. Yu and H. J. Qi, *Soft Matter*, 2017, **13**, 5558–5568.
5 W. Liu, L. X. Guo, B. P. Lin, X. Q. Zhang, Y. Sun and H. Yang, *Macromolecules*, 2016, **49**, 4023–4030.
6 H. Zeng, P. Wasylczyk, D. S. Wiersma and A. Priimagi, *Adv. Mater.*, 2018, **30**, 1–9.
7 T. Okamoto, K. Urayama and T. Takigawa, *Soft Matter*, 2011, **7**, 10585–10589.
8 S. K. Ahn, T. H. Ware, K. M. Lee, V. P. Tondiglia and T. J. White, *Adv. Funct. Mater.*, 2016, **26**, 5819–5826.
9 H. Jiang, C. Li and X. Huang, *Nanoscale*, 2013, **5**, 5225.
10 A. Agrawal, H. Chen, H. Kim, B. Zhu, O. Adetiba, A. Miranda, A. Cristian Chipara, P. M. Ajayan, J. G. Jacot and R. Verduzco, *ACS Macro Lett.*, 2016, **5**, 1386–1390.
11 V. Gimenez-Pinto, F. Ye, B. Mbanga, J. V. Selinger and R. L. Selinger, *Sci. Rep.*, 2017, **7**, 1–7.
12 H. Zeng, O. M. Wani, P. Wasylczyk, R. Kaczmarek and A. Priimagi, *Adv. Mater.*, 2017, **29**, 1–7.
13 W. J. Gies, *J. Dent. Res.*, 1928, **8**, 43–71.
14 Y. Gao, T. Mori, S. Manning, Y. Zhao, A. D. Nielsen, A. Neshat, A. Sharma, C. J. Mahnen, H. R. Everson, S. Crotty, R. J. Clements, C. Malcuit and E. Hegmann, *ACS Macro Lett.*, 2016, **5**, 4–9.
15 K. Urayama, *Macromolecules*, 2007, **40**, 2277–2288.
16 C. Ohm, M. Brehmer and R. Zentel, *Adv. Mater.*, 2010, **22**, 3366–3387.
17 A. Konya, V. Gimenez-Pinto and R. L. B. Selinger, *Front. Mater.*, 2016, **3**, 1–7.
18 D. Martella and C. Parmeggiani, *Chem. - A Eur. J.*, 2018, **24**, 12206–12220.
19 M. E. Prévôt, S. Ustunel and E. Hegmann, *Materials (Basel).*,

2018, **11**, year.

20 M. Yamada, M. Kondo, J. I. Mamiya, Y. Yu, M. Kinoshita, C. J. Barrett and T. Ikeda, *Angew. Chemie - Int. Ed.*, 2008, **47**, 4986–4988.

21 O. M. Wani, H. Zeng and A. Priimagi, *Nat. Commun.*, 2017, **8**, 1–7.

22 H. Zeng, O. M. Wani, P. Wasylczyk and A. Priimagi, *Macromol. Rapid Commun.*, 2018, **39**, 1–6.

23 A. H. Gelebart, D. Jan Mulder, M. Varga, A. Konya, G. Vantomme, E. W. Meijer, R. L. Selinger and D. J. Broer, *Nature*, 2017, **546**, 632–636.

24 H. Tian, Z. Wang, Y. Chen, J. Shao, T. Gao and S. Cai, *ACS Appl. Mater. Interfaces*, 2018, **10**, 8307–8316.

25 H. Shahsavan, S. M. Salili, A. Jákli and B. Zhao, *Adv. Mater.*, 2015, **27**, 6828–6833.

26 Jürgen Küpfer and H. Finkelmann, *Die Makromol. Chemie, Rapid Commun.*, 1991, **12**, 717–726.

27 Z. Pei, Y. Yang, Q. Chen, E. M. Terentjev, Y. Wei and Y. Ji, *Nat. Mater.*, 2014, **13**, 36–41.

28 C. M. Yakacki, M. Saed, D. P. Nair, T. Gong, S. M. Reed and C. N. Bowman, *RSC Adv.*, 2015, **5**, 18997–19001.

29 M. Warner and E. M. Terentjev, *Liquid Crystal Elastomers*, Oxford University Press, Oxford, England, 2003.

30 A. Agrawal, P. Luchette, P. Palffy-Muhoray, S. L. Biswal, W. G. Chapman and R. Verduzco, *Soft Matter*, 2012, **8**, 7138.

31 F. Greco, V. Domenici, A. Desii, E. Sinibaldi, B. Zupančič, B. Zalar, B. Mazzolai and V. Mattoli, *Soft Matter*, 2013, **9**, 11405.

32 R. R. Kohlmeyer and J. Chen, *Angew. Chemie - Int. Ed.*, 2013, **52**, 9234–9237.

33 J. M. Boothby and T. H. Ware, *Soft Matter*, 2017, **13**, 4349–4356.

34 J. J. Wie, K. M. Lee, T. H. Ware and T. J. White, *Macromolecules*, 2015, **48**, 1087–1092.

35 H. Zeng, D. Martella, P. Wasylczyk, G. Cerretti, J. C. G. Lavocat, C. H. Ho, C. Parmeggiani and D. S. Wiersma, *Adv. Mater.*, 2014, **26**, 2319–2322.

36 G. Babakhanova, T. Turiv, Y. Guo, M. Hendrikx, Q. H. Wei, A. P. Schenning, D. J. Broer and O. D. Lavrentovich, *Nat. Commun.*, 2018, **9**, 1–9.

37 S. J. Abhoff, F. Lancia, S. Iamsaard, B. Matt, T. Kudernac, S. P. Fletcher and N. Katsonis, *Angew. Chemie - Int. Ed.*, 2017, **56**, 3261–3265.

38 S. Iamsaard, S. J. Aßhoff, B. Matt, T. Kudernac, J. J. Cornelissen, S. P. Fletcher and N. Katsonis, *Nat. Chem.*, 2014, **6**, 229–235.

39 H. Shahsavan, S. M. Salili, A. Jakli and B. Zhao, *Adv. Mater.*, 2017, **29**, 1–7.

40 P. Plucinsky, M. Lemm and K. Bhattacharya, *Phys. Rev. E*, 2016, **94**, 1–5.

41 H. Aharoni, Y. Xia, X. Zhang, R. D. Kamien and S. Yang, *Proc. Natl. Acad. Sci.*, 2018, **115**, 7206–7211.

42 T. H. Ware, M. E. McConney, J. J. Wie, V. P. Tondiglia and T. J. White, *Science (80-.).*, 2015, **347**, 982–984.

43 M. E. McConney, A. Martinez, V. P. Tondiglia, K. M. Lee, D. Langley, I. I. Smalyukh and T. J. White, *Adv. Mater.*, 2013, **25**, 5880–5885.

44 A. Kotikian, R. L. Truby, J. W. Boley, T. J. White and J. A. Lewis, *Adv. Mater.*, 2018, **30**, 1–6.

45 C. P. Ambulo, J. J. Burroughs, J. M. Boothby, H. Kim, M. R. Shankar and T. H. Ware, *ACS Appl. Mater. Interfaces*, 2017, **9**, 37332–37339.

46 H. Aharoni, E. Sharon and R. Kupferman, *Phys. Rev. Lett.*, 2014, **113**, 1–5.

47 B. A. Kowalski, C. Mostajeran, N. P. Godman, M. Warner and T. J. White, *Phys. Rev. E*, 2018, **97**, 1–5.

48 Z. L. Wu, M. Moshe, J. Greener, H. Therien-Aubin, Z. Nie, E. Sharon and E. Kumacheva, *Nat. Commun.*, 2013, **4**, 1586–1587.

49 C. Ahn, X. Liang and S. Cai, *Extrem. Mech. Lett.*, 2015, **5**, 30–36.

50 L. Yu, H. Shahsavan, G. Rivers, C. Zhang, P. Si and B. Zhao, *Adv. Funct. Mater.*, 2018, **28**, 1802809.

51 R. D. Andrews, A. V. Tobolsky and E. E. Hanson, *J. Appl. Phys.*, 1946, **17**, 352–361.

52 L. G. Baxandall and S. F. Edwards, *Macromolecules*, 1988, **21**, 1763–1772.

53 A. S. Aprem, K. Joseph and S. Thomas, *J. Appl. Polym. Sci.*, 2004, **91**, 1068–1076.

54 S. Kaang, D. Gong and C. Nah, *J. Appl. Polym. Sci.*, 1997, **65**, 917–924.

55 P. J. Flory, *Trans. Faraday Soc.*, 1960, **56**, 722–743.

56 N. K. Singh and A. J. Lesser, *Macromolecules*, 2011, **44**, 1480–1490.

57 D. R. Rottach, J. G. Curro, G. S. Grest and A. P. Thompson, *Macromolecules*, 2004, **37**, 5468–5473.

58 Y. Meng, J. Jiang and M. Anthamatten, *ACS Macro Lett.*, 2015, **4**, 115–118.

59 J. Zhou and S. S. Sheiko, *J. Polym. Sci. Part B Polym. Phys.*, 2016, **54**, 1365–1380.

60 A. Lendlein, H. Jiang, O. Junger and R. Langer, *Nature*, 2005, **434**, 879–882.

61 Q. Zhao, H. J. Qi and T. Xie, *Prog. Polym. Sci.*, 2015, **49-50**, 79–120.

62 S. Schauer, T. Meier, M. Reinhard, M. Röhrig, M. Schneider, M. Heilig, A. Kolew, M. Worgull and H. Hölscher, *ACS Appl. Mater. Interfaces*, 2016, **8**, 9423–9430.

63 T. Meier, J. Bur, M. Reinhard, M. Schneider, A. Kolew, M. Worgull and H. Hölscher, *J. Micromechanics Microengineering*, 2015, **25**, 065017.

64 M. Deutsch, *Phys. Rev. A*, 1991, **44**, 8264–8270.

65 P. Davidson, D. Petermann and A. M. Levelut, *J. Phys. II*, 1995, **5**, 113–131.

66 M. O. Saed, A. H. Torbati, C. A. Starr, R. Visvanathan, N. A. Clark and C. M. Yakacki, *J. Polym. Sci. Part B Polym. Phys.*, 2017, **55**, 157–168.

67 A. Agrawal, A. C. Chipara, Y. Shamoo, P. K. Patra, B. J. Carey, P. M. Ajayan, W. G. Chapman and R. Verduzco, *Nat. Commun.*,

2013, **4**, 1739.

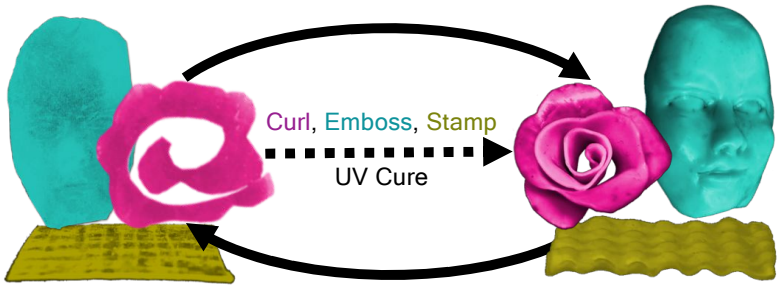

Optimization of the double network structure of LCE enables complex shape programming